A Copolymer-in-Oil Tissue-Mimicking Material With Tuneable Acoustic and Optical Characteristics for Photoacoustic Imaging Phantoms

Lina Hacker, James Joseph, Aoife M. Ivory, Mohand O. Saed, Bajram Zeqiri, Srinath Rajagopal, and Sarah E. Bohndiek

***Abstract*— Photoacoustic imaging (PAI) standardisation demands a stable, highly reproducible physical phantom to enable routine quality control and robust performance evaluation. To address this need, we have optimised a low-cost copolymer-in-oil tissue-mimicking material formulation. The base material consists of mineral oil, copolymer and stabiliser with defined Chemical Abstract Service numbers. Speed of sound $c(f)$ and acoustic attenuation coefficient α (f) were characterised over 2–10 MHz; optical absorption $\mu_a(\lambda)$ and reduced scattering $\mu_s'(\lambda)$ coefficients over 450–900 nm. Acoustic properties were optimised by modifying base component ratios and optical properties were adjusted using additives. The temporal, thermomechanical and photo-stability were studied, along with intra-laboratory fabrication and field-testing. $c(f)$ could be tuned up to (1516±0.6)m·s^{-1} and α (f) to (17.4±0.3)dB·cm^{-1} at 5 MHz. The base material exhibited negligible $\mu_a(\lambda)$ and $\mu_s'(\lambda)$, which could be independently tuned by addition of Nigrosin or TiO_2 respectively. These properties were stable over almost a year and were minimally affected by recasting. The material showed high intra-laboratory reproducibility (coefficient of variation <4% for $c(f)$, $\alpha(f)$, optical transmittance and reflectance), and good photo- and mechanical-stability in the relevant working range (20–40°C). The optimised copolymer-in-oil material represents an excellent candidate for widespread application in PAI phantoms, with properties suitable for broader use in biophotonics and ultrasound imaging standardisation efforts.**

***Index Terms*— Copolymer-in-oil, phantom, photoacoustic imaging, SEBS, standardization.**

Manuscript received April 16, 2021; revised May 31, 2021; accepted May 31, 2021. Date of publication June 21, 2021; date of current version November 30, 2021. This work was supported by Cancer Research UK under Grant C14303/A17197, Grant C9545/A29580, Grant C47594/A16267, and Grant C197/A16465. The work of Lina Hacker was supported by the NPL's MedAccel Programme through the Department for Business, Energy and Industrial Strategy's Industrial Strategy Challenge Fund. *(Corresponding author: Sarah E. Bohndiek.)*

Lina Hacker and Sarah E. Bohndiek are with the Department of Physics, University of Cambridge, Cambridge CB3 0HE, U.K., and also with the Cancer Research UK Cambridge Institute, University of Cambridge, Cambridge CB2 0RE, U.K. (e-mail: lh592@cam.ac.uk; seb53@cam.ac.uk).

James Joseph was with the Department of Physics, University of Cambridge, Cambridge CB3 0HE, U.K. He is now with the School of Science and Engineering, University of Dundee, Dundee DD1 4HN, U.K. (e-mail: jjoseph001@dundee.ac.uk).

Aoife M. Ivory, Bajram Zeqiri, and Srinath Rajagopal are with the Ultrasound and Underwater Acoustics Group, Department of Medical, Marine and Nuclear Physics, National Physical Laboratory (NPL), Teddington TW11 0LW, U.K. (e-mail: aoife.ivory@npl.co.uk; bajram.zeqiri@npl.co.uk; srinath.rajagopal@npl.co.uk).

Mohand O. Saed is with the Department of Physics, University of Cambridge, Cambridge CB3 0HE, U.K. (e-mail: mos29@cam.ac.uk).

This article has supplementary downloadable material available at https://doi.org/10.1109/TMI.2021.3090857, provided by the authors.

Digital Object Identifier 10.1109/TMI.2021.3090857

I. Introduction

PHOTOACOUSTIC imaging (PAI) is an emerging biomedical imaging modality that reveals the spatial distribution of optical absorption in tissue through the photoacoustic effect [1], [2]. PAI has now matured into early clinical trials for indications ranging from oncology to inflammatory disease [3]–[6]. Establishing the precision and accuracy of new optical-imaging biomarkers through technical validation [7], [8] is vital for successful translation from research and development to adoption in healthcare systems. Such technical validation studies are often performed using a stable physical phantom to firstly, enable robust performance evaluation for comparison of different instruments and secondly, to underpin quality control for routine use. Ideally, such a PAI phantom should be: (1) tissue-mimicking in terms of tuneable acoustic and optical properties; (2) mechanically robust; (3) stable over time; (4) simple and highly reproducible to manufacture; (5) flexible in geometry and architecture; (6) non-toxic; (7) made with ingredients widely available from scientific suppliers; and finally, (8) low cost. At present, PAI lacks a widely-accepted phantom that meets all of these requirements.

A wide range of materials have already been proposed as PAI phantom candidates, including: hydrogels [9], [10]; polyvinyl alcohol (PVA) [11]–[14]; polyvinyl chloride plastisol (PVCP) [15]–[21]; silicone [22], [23]; and resin-based materials [24], [25]. Nonetheless, for all these materials certain drawbacks exist that limit their application as a durable PAI phantom material. Hydrogels, for example, are susceptible to mechanical damage, dehydration and bacterial growth in storage and therefore have a limited shelf life [26]–[28]. The

longevity can be increased by careful handling or addition of chemicals, but common preservatives, such as formaldehyde [29] or benzalkonium chloride [30], are highly hazardous and require cautionary measures during fabrication and handling, especially in a clinical environment. Moreover, encapsulation of targets containing water-soluble dyes is required to prevent their diffusion within the base material. PVA cryogels exhibit higher structural rigidity and longevity than hydrogels, but their shelf-life is also limited and their preparation process involves long freeze-thaw cycles [31]. Slight variations in these cycles can lead to inhomogeneities [11], compromising reproducibility, and independent tunability of acoustic and optical parameters is limited [32]. Resin-based materials and silicone are characterized by unnatural speed of sound and/or acoustic attenuation [28], [33], [34] which are unrepresentative of soft tissue. PVCP has a non-trivial fabrication process with high preparation temperatures up to 180-220°C [16], [18], [19], [35]. Moreover, there is a lack of a supply chain with scientific suppliers [17] and some plasticizers are based on phthalates, which can act as reproductive and developmental toxicants [36].

Recently, new materials based on copolymer-in-oil compositions have been reported, such as gel wax [37]–[40] or mixtures based on thermoplastic styrenic elastomers, such as polystyrene-block-poly(ethylene-ran-butylene)-block-polystyrene (SEBS) [41]–[43], [67]. Thermoplastic elastomers are composed of a rigid phase made of styrene structures and a rubber phase made of elastomeric structures and are easily processable as a melt at elevated temperatures [44]. Copolymer-in-oil materials are characterized by acoustic and optical properties similar to soft tissue and have good longitudinal stability [40]–[43]. Fortunately, they are also cost-effective, non-water absorbing, non-toxic and biologically inert [41], [42], although recipes based on commercial polymer or gel wax [37], [41] result in high batch-to-batch variation, impairing the reproducibility of the phantom fabrication. Moreover, copolymer-in-oil materials can be highly thermosensitive and the reported tunability of the acoustic properties is currently limited to 1480 $m{\cdot}s^{-1}$ [41] for speed of sound, which is lower than the ultrasound soft tissue standard of 1540 $m{\cdot}s^{-1}$ [45] (Supplementary Table I). While speed of sound can be increased by using oil with increased viscosity [42] or employing additives such as paraffin wax [38] or glycerol [67], these can result in high acoustic attenuation [38], [42] or backscattering [67]. Low density polyethylene [40], [41] has been employed as a tuning agent, but a comprehensive comparison of different polyethylene types has not yet been performed.

To overcome these limitations, we have optimised a copolymer-in-oil formulation for use as a tissue-mimicking phantom material for PAI, which has a facile manufacturing process, with all ingredients being low-cost, having defined Chemical Abstracts Service (CAS) numbers, and being readily available from standard scientific suppliers. Firstly, we show that the phantom material can provide independently tuneable, tissue-mimicking characteristics in the relevant optical excitation and acoustic detection ranges for biomedical PAI. Secondly, we demonstrate that the material exhibits sufficient photo-, thermomechanical- and longitudinal- stability for short- and long-term precision studies. Finally, we demonstrate the suitability of the material to create phantoms of different architectures for mesoscopic and macroscopic PAI instruments. By fulfilling the aforementioned criteria for an ideal PAI phantom, the developed material could facilitate PAI technical validation studies and represents an excellent candidate for future routine quality control in preclinical and clinical PAI applications.

II. Methods

A. Phantom Fabrication

A summary of the phantom material compositions used for the acoustic study can be found in Supplementary Table II and for the optical study in Supplementary Table III. In order to reduce batch-to-batch variability, all specified components have defined CAS numbers and are readily available from large scientific suppliers. For the acoustic study the following thermoplastic elastomers were tested: high molecular weight (MW) SEBS (Sigma Aldrich 200557-250G), SEBS-graft maleic anhydride (Sigma Aldrich 432431-250G), low MW SEBS (Sigma Aldrich 200565-250G) and Polystyrene-block-polybutadiene-block-polystyrene (SBS, Sigma Aldrich 182877-250G). Moreover, the following polyolefins were tested in order to increase the mechanical stability of the base material: Low-density Polyethylene (LDPE, Alfa Aesar 43949.30), Polystyrene (Sigma Aldrich 182427-500G), Polypropylene (Sigma Aldrich 427888-1KG), high MW Polyethylene (Sigma Aldrich 427772-250g), linear LDPE (Sigma Aldrich 428078-1KG), low MW Polyethylene (Sigma Aldrich 427795-250g) and high-density Polyethylene (HDPE, Sigma Aldrich 427985-1KG). Mineral oil (Sigma Aldrich-330779-1L) was used as a base with a viscosity of 14.20 - 17.00 $mm^2{\cdot}s^{-1}$ at 40°C, a speed of sound of 1440 $m{\cdot}s^{-1}$ and a density of 0.838 $g{\cdot}mL^{-1}$ at 25 °C. Information on the optical absorption profile can be found in Supplementary Figure 1. 5 w/v% butylated hydroxytoluene (HT, Sigma Aldrich W218405-1KG-K) was added as an antioxidant to all samples to increase the stability of material and prevent discolouration of SEBS at high temperatures [46]. After optimization, remaining studies combined a representative concentration of 30 w/v% high MW SEBS with 8 w/v% LDPE. Titanium Dioxide (TiO_2, Sigma Aldrich 232033-100g) was added to provide optical scattering and alcohol-soluble Nigrosin (Sigma Aldrich 211680-100G) to provide optical absorption. To increase the accuracy of the optical adjustment, a working stock solution of Nigrosin in mineral oil (2.5 mg/ml) was prepared. The fabrication can be summarized in six steps (Figure 1):

1. All components are weighed and the optical scattering (TiO_2) and absorbing agents (e.g. Nigrosin) are added to the mineral oil in a glass beaker.
2. For homogenous distribution within the base phantom matrix, the mixture is sonicated at 90°C (sonication frequency: 44 kHz) until the scattering and absorbing agents are dissolved and no aggregates are visually detectable (60-90 mins).

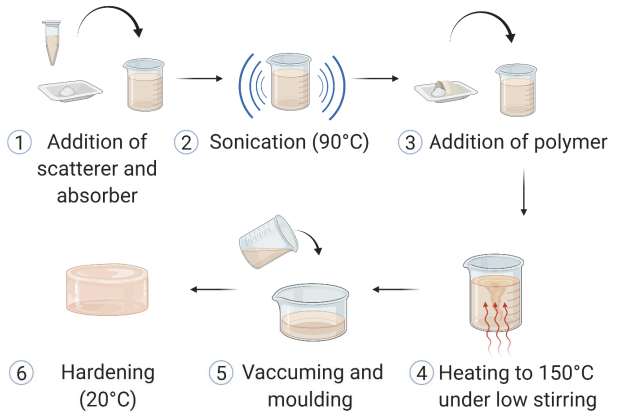

Fig. 1. **Fabrication and characterization of the copolymer in oil-material**. The six-step fabrication procedure of the copolymer-in-oil material is displayed. (1) Materials for optical scattering and absorption are added to mineral oil and (2) sonicated at 90°C until dissolved. (3) Polymer(s) and stabilizer are added, and (4) the mixture is heated up in an oil bath to 150°C under low stirring. (5) Upon dissolution of all components, the sample is poured in a suitable phantom mould and (6) left to harden at room temperature. Created with BioRender.

3. Polymers and stabilizer are added to the mineral oil solution in their respective ratios.
4. The complete mixture is heated up to 150°C in an oil bath under low stirring conditions (150 rpm) until all components are dissolved and no aggregates are visually detectable. If the polymer appears to float over the oil, the mixture is manually stirred using a metallic spatula.
5. The solution is vacuumed for removal of air bubbles in a vacuum chamber for 3-5 minutes and then carefully poured from low height into a suitable phantom mould. Alternatively, a vacuum oven (Gallenkamp D8B, Germany, 30 mins at 120° C (248F) and 30 inches/Hg pressure) can be used.
6. Once set, samples may be stored at room temperature.

B. Acoustic Characterization

The frequency-dependent speed of sound, $c(f)$, and acoustic attenuation, $\alpha(f)$, were evaluated using a broadband through-transmission substitution method employing the materials acoustic characterisation facility at the National Physical Laboratory (NPL), UK [47] (Supplementary Figure 2A,B). A 10 MHz centre frequency ultrasound transducer of active element diameter 10 mm (Force Technology, Brondby, Denmark) was placed within a water tank filled with de-ionised water and driven by an Olympus 5073PR pulser–receiver (Olympus NDT, Waltham, MA, USA). A broadband hydrophone (30 mm active element diameter bilaminar membrane hydrophone, GEC Marconi) was used for detection. Waveforms were acquired using a DPO 7254 oscilloscope (Tektronix UK, Bracknell, UK).

Four acoustic pulses were acquired in each measurement set: a reference through-water pulse with no sample present in the acoustic path; a through-sample transmission; together with acoustic reflections received at the transmitter from the front and rear surfaces of the sample.

To assess the inherent measurement system uncertainty, four measurements were taken per sample, in which pulse energy, damping and the transducer-sample distance (up to 5 mm) was varied, making the measurements independent of these variables. The sample average and standard error of the mean (SEM) of the four measurements per sample were then calculated. The system-specific Type B effects on the measurements are reviewed elsewhere [48]. Circular samples of a diameter of 7 cm and a thickness ranging between 6 and 9 mm were prepared for acoustic testing. The water tank temperature was recorded immediately before measurements on any test sample using a UKAS-calibrated IP 39C spirit-in-glass thermometer (G. H. Zeal, London, UK).

The Transmission Loss (TL) of a given sample (expressed in $\mathrm{dB{\cdot}cm^{-1}}$) at the frequency f was calculated using the expression [48]:

$$TL(f) = -\frac{20}{d}\log_{10}\left[\frac{U_s(f)}{U_w(f)}\right] + \alpha_{\mathrm{w}}(f), \tag{1}$$

where d is the sample thickness (in cm), $U_{\mathrm{w}}(f)$ and $U_{\mathrm{s}}(f)$ are the respective voltage magnitude spectra of the through-water and through-sample pulse, and $\alpha_{\mathrm{w}}(f)$ is the attenuation coefficient of ultrasound (in $\mathrm{dB{\cdot}cm^{-1}}$) of pure water at the specific water tank temperature [49]. To remove the influence of interfacial losses in calculating the frequency-dependent attenuation coefficient ($\alpha_i(f)$) of the material, two thicknesses $\mathrm{d_1}$ and $\mathrm{d_2}$ ($\mathrm{d_2} > \mathrm{d_1}$) of a representative sample were taken and the acoustic attenuation was calculated using the two-sample substitution technique [48]:

$$\alpha_i(f) = -\frac{20}{d_2 - d_1}\left(\log_{10}\left[\frac{U_{s2}(f)}{U_{w2}(f)}\right] - \log_{10}\left[\frac{U_{s1}(f)}{U_{w1}(f)}\right]\right) + \alpha_{\mathrm{w}}(f) \tag{2}$$

For the most promising material recipe, the attenuation accounting for the interfacial losses was assessed, finding that the impact of the interfacial losses is negligible. The speed of sound $c(f)$ (in $\mathrm{m{\cdot}s^{-1}}$) was calculated using the expression [48]

$$c(f) = c_w\left[1 + 2 * \frac{\theta_w(f) - \theta_s(f)}{\theta_2(f) - \theta_1(f)}\right], \tag{3}$$

where c_w depicts the temperature dependent speed of sound of water and, $\theta_1(f)$, $\theta_2(f)$, $\theta_{\mathrm{w}}(f)$ and $\theta_{\mathrm{s}}(f)$ the corresponding unwrapped phase spectra of the front-reflected, back-reflected, through-water and through-sample voltage pulses.

C. Optical Characterization

An in-house double-integrating-sphere (DIS) system based on the system developed by Pickering *et al.* [50] (Supplementary Figure 2C,D) was used to determine the optical absorption (μ_{a}) and reduced scattering coefficients (μ'_{s}) of the material samples. The system is composed of two integrating spheres (Avantes, AvaSphere-50, 50 cm internal diameter) between which the sample is placed. Each integrating sphere is connected to a spectrometer (Avantes, Starline Avaspec-2048) via an optical fibre. The reflectance sphere is connected to a light source (Avantes, Avalight-HAL-s-mini) via a third optical fibre. The measured transmission and reflectance values are recorded and entered into the inverse adding doubling (IAD)

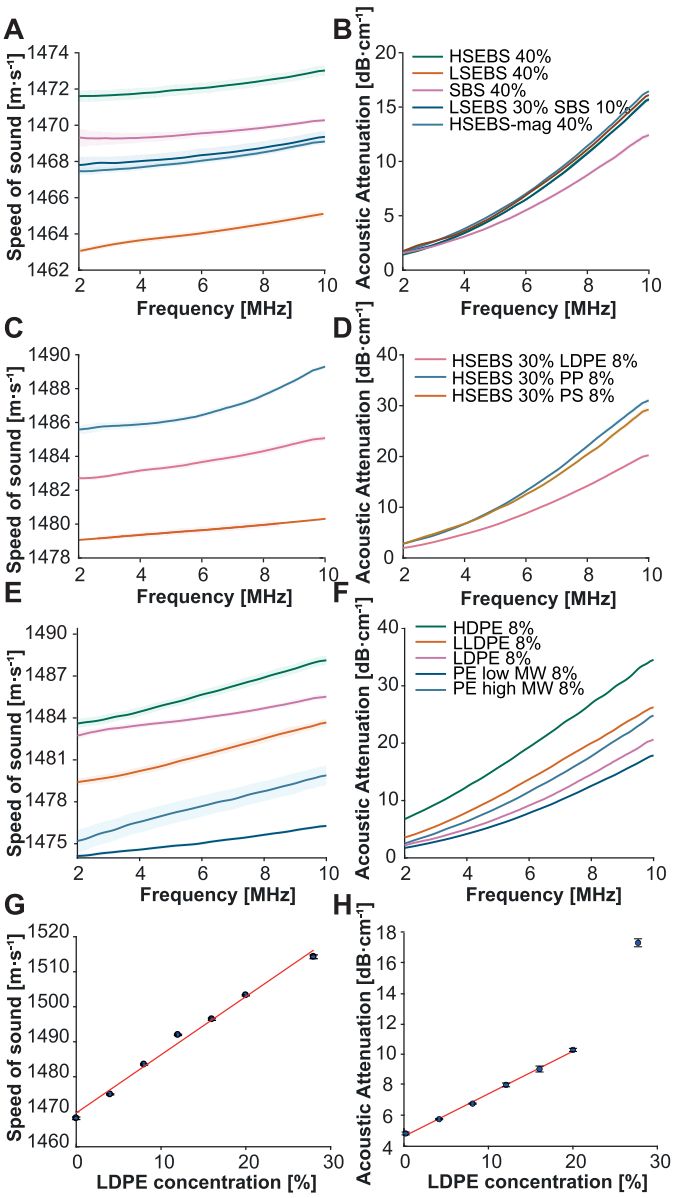

Fig. 2. **Comparison of speed of sound and acoustic attenuation coefficient of samples composed of different polymer types.** The speed of sound (A) and acoustic attenuation coefficient (B) for samples composed of mineral oil containing 40 w/v% high and low MW SEBS (HSEBS = green, LSEBS = yellow), SBS (pink), SEBS-graft-maleic anhydride (HSEBS-mag = light blue) and one sample composed of 30 w/v% low MW SEBS and 10 w/v% SBS (dark blue) in a frequency range of 2 to 10 MHz. After selecting high MW SEBS for further study, the speed of sound (C) and acoustic attenuation coefficient (D) were then evaluated for samples composed of mineral oil containing 30 w/v% high MW SEBS, and a second polymer at 8 w/v%, which was either (low density) polyethylene (LDPE = pink), polystyrene (PS = yellow), or polypropylene (PP = blue). After identifying LDPE (pink) as a suitable candidate, the speed of sound (E) and acoustic attenuation (F) of different types of polyethylene (PE) were compared, including: high density polyethylene (HDPE, green), linear LDPE (LLDPE, yellow), low MW PE (dark blue) and high MW PE (light blue; all at 8 w/v%). Finally, the speed of sound (E; $R^2 = 0.9862$; $f(x) = 1.662 \cdot x + 1470$; SSE = 21.6214) and acoustic attenuation coefficient (F; $R^2 = 0.9980$; $f(x) = 0.276 \cdot x + 4.65$; SSE = 0.0450) at 5 MHz were evaluated for samples composed of mineral oil containing 30 w/v% high MW SEBS and increasing LDPE concentration. For all panels, data is shown as mean ± SEM for n = 4 measurements per sample (error bars given as shaded area in A-F or explicit error bars in G, H; if not visible, errors are contained within the line or point).

program (Source code: http://omlc.org/software/iad/) [51] to estimate the optical properties of the material. The IAD algorithm iteratively searches for a solution to the radiative transfer equation by assuming layered samples with homogeneous optical properties and uniform light illumination. Rectangular samples with a width of 5.9 cm, a height of 1.8 cm and a thickness ranging between 2 and 3 mm were prepared for optical testing. Sample thicknesses were determined before each measurement using vernier callipers. Based on previous reports on a similar material type (gel wax), the scattering anisotropy factor (g) was taken to be g = 0.7 and the refractive index n = 1.4 [39]. Three measurements at distinct positions on the sample were taken in a wavelength range of 450 to 900 nm. Compression of the sample can impact the measurements [51]. To minimize this influence, the reflectance sphere was placed on a motorized stage (Thorlabs MTS50) to accurately control the distance between the spheres. The stage was set to zero at the position where the integrating spheres were perfectly aligned and the set distance was then adjusted according to the measured sample thickness.

D. Stability Studies

Photo-, thermomechanical and longitudinal stability of the acoustic and optical properties were tested on representative phantoms composed of 30 w/v% high MW SEBS, 8 w/v% LDPE, 0.03 w/v% TiO_2 and 300 μL Nigrosin stock solution. A consistent PAI readout from the phantom requires good photostability. Thermomechanical stability was assessed as materials based on thermoplastic elastomers exhibit temperature sensitive viscoelastic properties [44] and stability over the relevant working range (20-40 °C) is important. Finally, longitudinal stability of the phantom acoustic and optical properties was assessed regularly over a time frame of eleven months. It should be noted that while an assessment of the thermoelastic Grüneisen parameter was not conducted in this study, a detailed characterization in a similar material was recently reported by Bakaric *et al.* [52].

1) Photostability: To assess the photostability of the phantom material, a cylindrical phantom (length: 40 mm, diameter: 28 mm) was fabricated from the stated composition and placed within a commercial photoacoustic tomography instrument (MSOT inVision 256-TF; iThera Medical GmbH), described in detail elsewhere [53]. Excitation pulses were provided by a tunable (660–1300 nm) optical parametric oscillator (OPO), pumped by a nanosecond (ns) pulsed Nd:YAG laser (10 Hz repetition rate up to 7 ns pulse duration). A custom optical fibre assembly creates a diffuse ring of uniform illumination over the imaging plane within the sample. The sample is coupled to the transducers using heavy water in a water bath. For ultrasound detection, 256 toroidally focused ultrasound transducers covering an angle of 270° are used (centre frequency of 5 MHz, 60% bandwidth) allowing tomographic reconstruction.

To assess the photostability, a fixed position within the phantom was irradiated with 17,500 laser pulses over a time period of 30 minutes using wavelengths between 660 and 850 nm

in 10 nm steps. Data analysis was performed using ViewMSOT software (v3.6.0.119; iThera Medical GmbH). Model–based image reconstruction was applied and the mean photoacoustic signal within a region of interest (ROI) drawn around the circular cross section of the phantom was quantified.

2) Thermal Stability: The degradation characteristics of the material were determined by thermal gravimetric analysis (TGA). TGA was performed using a Thermal Analysis TG Q500 instrument (TA instruments, New Castle, DE, USA). Sample measurements (sample weight approximately 4 mg) were conducted in the temperature range from 25 to 300 °C at a heating rate of 5 °C min^{-1}. The temperature at 5 % of mass loss was determined using universal analysis software (TA instruments, USA).

3) Thermo-Mechanical Stability: The viscoelastic properties of the material were analysed by conducting a dynamic mechanical analysis (DMA) using DMAQ850 instrument (TA instruments, New Castle, DE, USA). Length, width and thickness of the sample were measured using vernier callipers (approximate size: 30 (length) × 10 (width) × 5 (thickness) mm^3). Samples were tested in tensile mode, with the active length measuring approximately 15 mm. A strain of 0.01 (1%) was applied to the sample at a frequency of 1 Hz while the temperature was increased from −100 to +100 °C at a rate of 3 °C·min^{-1}. The glass transition temperature (Tg) was measured at the peak of tan delta and the plastic flow temperature (Tf) was marked by the drop of the storage modulus to zero. The loss modulus, storage modulus and tan(δ) were recorded using the TA instruments TRIOS software (v 5.0.0). The loss modulus (E") refers to the energy loss due to the viscous response of the material, whereas the storage modulus (E') refers to the energy storage caused by the elastic response of the material. The vectoral addition of these two moduli is the complex modulus (E^*) [54], [55]

$$E^* = \sqrt{E''^2 + E'^2} \tag{4}$$

which can be regarded as the Young's modulus (E) in Hookean materials such as biological soft tissues [56], [57].

E. Photoacoustic Imaging

Photoacoustic imaging was performed using the tomography system described above and a commercial photoacoustic mesoscopy system (RSOM Explorer P50; both iThera Medical GmbH, München, Germany), described in detail elsewhere [58]. In the mesoscopy system, laser light is generated by a 532 nm laser (pulses: 1 ns; ≤ 1 mJ/pulse) and delivered through a customized 2-arm fibre bundle (spot size: 3.5 × 5 mm). Photoacoustic signals are detected by a spherically focused $LiNbO_3$ detector (center frequency: 50 MHz; bandwidth: 10 - 90 MHz; focal diameter: 3 mm; focal distance: 3 mm; f-number: 1). The recorded data is amplified by a low noise amplifier of 63 dB gain. The scanning head is attached to two motorised stages and coupled to the sample surface by an interchangeable water-filled (2 mL) interface.

The base material of the phantoms was composed of 30 w/v% high MW SEBS, 8 w/v% LDPE, 0.03 w/v% TiO_2 and 0.0007 w/v% Nigrosin. For the mesoscopic system, stainless steel was used to create a heat-resistant rectangular phantom mould of the following dimensions: length: 50 mm, width: 50 mm, height: 7 mm. For imaging targets, three red fibres (diameter: 126 μm, smilco) were positioned at different depths (0.5, 1.5 and 2.5 mm). These demonstrate the use of our base material combined with user-selected targets of a different material. Although the fibres were not purchased from a large scientific supplier, after testing of different types of targets (e.g. wires, sutures and threads), we found that they presented the best compromise for an appropriate size target without introducing artefacts. For the tomographic system, a heat-resistant cylindrical glass phantom mould (diameter: 28 mm) was fabricated out of an open-top 50 ml glass syringe (Sigma-Aldrich, CADG5157). Two equally distanced stainless-steel rods (diameter: 4 mm; rod-rod distance: 10 mm) on a Polytetrafluoroethylene (PTFE) base were inserted into the glass mould. The moulds were filled with the copolymer-in oil material until the phantoms reached a length of 50 mm. After hardening, the phantoms were removed from the mould and the inclusions were filled, demonstrating a phantom where both the background matrix and target inclusions are formed of the same copolymer-in-oil base. For the inclusion material, a green oil-soluble dye was chosen (0.04 w/v%, GRC 43104, Caligo safe wash relief inks, Cranfield Colours, Cwmbran, UK) due to its absorbing properties in the first near infra-red window [37] and suspended in the base material.

For the RSOM image acquisition, the phantom was placed underneath the water-filled interface covering the scan head. For coupling of the phantom to the interface, degassed commercial ultrasound gel (Aquasonic Clear, Parker Labs) was used. Images were acquired over a field of view of 12 × 12 mm (step size: 20 μm) at 85% laser energy. For the MSOT image acquisition, the same sample preparations were used as in our standard operating procedure for *in vivo* imaging [58] to make our *in vivo* and *in vitro* imaging approach as comparable as possible. This involved wrapping the phantom in a thin polyethylene membrane using degassed commercial ultrasound gel as a coupling medium and inserting it into the supplied holder (iThera Medical). The holder was then immersed in degassed heavy water maintained at 34°C within the MSOT system. After a stabilisation period of 15 minutes, images were acquired through the center of the phantom using the following wavelengths: 660 nm, 700 nm, 730 nm, 760 nm, 800 nm, 850 nm, 900 nm, 950 nm, 1040 nm (with an average of 10 pulses per wavelength).

F. Image and Statistical Analysis

Tomographic imaging data was reconstructed using a model-based algorithm and analysis was performed using ViewMSOT software (v3.6.0.119; iThera Medical GmbH). Mesoscopic imaging data was reconstructed using a beam-forming algorithm provided by the vendor (iThera Medical GmbH), which models the sensitivity field of the focused detector and generates 3-dimensional images. The subsequent images were analysed using MATLAB.

All measurements in the acoustic and optical characterisations were performed at least three times per sample. Statistical analysis was performed using Prism (GraphPad)

and MATLAB. All data are shown as mean ± SEM unless otherwise stated. The coefficient of variation (COV) was calculated as the ratio of the standard deviation (SD) to the mean, expressed as a percentage.

III. Results

A. Systematic Optimisation of Copolymer-in-Oil Materials Results in High Speed of Sound

We first sought to refine the copolymer-in-oil material composition to bring the speed of sound closer to the ultrasound soft tissue average, while keeping the acoustic attenuation close to tissue relevant values. To achieve this, we compared the acoustic performance of different base polymers of the material, which are thermoplastic styrenic elastomers. Phantoms were produced employing 40 w/v% low and high molecular weight (MW) SEBS, SEBS-graft-maleic anhydride and SBS, the dehydrogenated version of SEBS. A high percentage of polymer was chosen for these studies, since increasing the SEBS concentration has been shown to increase the speed of sound [42]. The sample containing high MW SEBS was characterized by the highest speed of sound (1471.9 ± 0.3 $m{\cdot}s^{-1}$ at 5 MHz, Figure 2A) whilst having similar attenuation values (Figure 2B) compared to the remaining polymers tested. Higher molecular weight usually leads to enhanced thermal and mechanical properties (e.g. increase in strength, toughness and chemical stress crack resistance), but also to higher stiffness due to higher chain entanglement and decreased molecular mobility [59]. Notably, the sample containing SBS had the lowest attenuation value (4.11 ± 0.11 $dB{\cdot}cm^{-1}$ at 5 MHz, Figure 2B), but as SBS is more susceptible to degradation at high temperatures and more prone to oxidation in the absence of antioxidants [44], we chose to focus on high MW SEBS as our base polymer. It is known that SEBS samples with low polymer concentrations are susceptible to plastic deformation [60]. Therefore, we aimed to strengthen the mechanical stability of the material by addition of a second polymer, which could also further improve the acoustic properties. We compared the acoustic performance of samples containing (low density) polyethylene (LDPE), polystyrene and polypropylene as additive second polymers.

Polypropylene gave the highest speed of sound within the tuning range (1486 ± 0.10 $m{\cdot}s^{-1}$ at 5 MHz, Figure 2C), but also the highest acoustic attenuation (9.27 ± 0.15 $dB{\cdot}cm^{-1}$ at 5 MHz, Figure 2D).

By comparison, the sample containing LDPE was considerably less attenuating (6.27 ± 0.12 $dB{\cdot}cm^{-1}$ at 5 MHz, Figure 2D) with a similar speed of sound (1482 ± 0.2 $m{\cdot}s^{-1}$ at 5 MHz, Figure 2C), which makes it preferable as a second polymer additive for our purposes. In order to identify the most suitable type of polyethylene, we compared the speed of sound (Figure 2E) and acoustic attenuation (Figure 2F) of different polyethylene subtypes, including: high density polyethylene (HDPE), linear LDPE (LLDPE), low MW PE and high MW PE (all at 8 w/v%). Here again, LDPE gave the most favourable characteristics. With LDPE identified as a suitable strengthening agent, we proceeded to tune the speed of sound of material samples with a set concentration

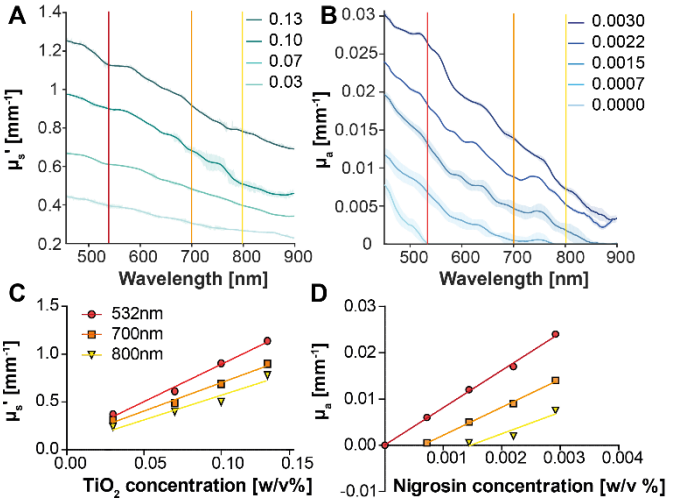

Fig. 3. **Independent tuning of the reduced scattering and optical absorption coefficients by variation of titanium dioxide and Nigrosin concentrations**. The (A) reduced scattering coefficient (μ_s') and (B) optical absorption coefficient (μ_a) of a material sample composed of 30 w/v% high MW SEBS and 8 w/v% LDPE were measured at a wavelength range of 450 to 900 nm at varying concentrations of TiO_2 and Nigrosin using the DIS system. The variation of μ_s' (C) and μ_a (D) with TiO_2 and Nigrosin content is plotted for common PAI wavelengths (indicated with vertical lines in A and B) of 532 nm (red), 700 nm (orange) and 800 nm (yellow). For all panels, data is shown as mean ± SEM for n = 3 measurements per sample (error bars given as shaded area in A, B; within symbols in C, D).

of 30 w/v% SEBS by variation of LDPE content. In this way, the speed of sound could be increased up to a value 1516 ± 0.65 $m{\cdot}s^{-1}$ (Figure 2G) at the expense of increasing acoustic attenuation to 17.3 ± 0.26 $dB{\cdot}cm^{-1}$ at 5 MHz (Figure 2H; Supplementary Table IV). For LDPE concentrations under 20 w/v%, the acoustic attenuation appeared to increase linearly (Figure 2H), with a more substantial increase in attenuation noted at 30 w/v%. Overall, the results suggest that the material would be suitable for mimicking the speed of sound of tissues such as breast fat and parenchyma (1450-1490 $m{\cdot}s^{-1}$), but still does not provide sufficient speed of sound for tissues such as skin, muscle, kidney or prostate (>1520 $m{\cdot}s^{-1}$; Supplementary Table I). For mimicking fatty tissues, LDPE concentrations under 8 w/v% are preferable, as the acoustic attenuation becomes too large otherwise.

B. Negligible Optical Absorption and Scattering of the Copolymer-in-Oil Material Facilitates Tuning of Optical Properties Through Additives

Next, we examined the optical properties of the fabricated material. We found that the optical absorption and scattering properties of the material increased slightly with LDPE concentration, however, even with one of the highest LDPE concentrations tested (20 v/w%) the samples showed negligible absorption at 800 nm and did not exceed a reduced scattering value of 0.24 mm^{-1}, which is still below the threshold of most soft tissues [61]. As a result, it was possible to tune the optical properties of the material through further additives. Using material incorporating 30 w/v% SEBS and 8 w/v% LDPE, a tissue-mimicking range of optical properties [62] were obtained through addition of TiO_2 (Figure 3A) or Nigrosin (Figure 3B) for reduced scattering and

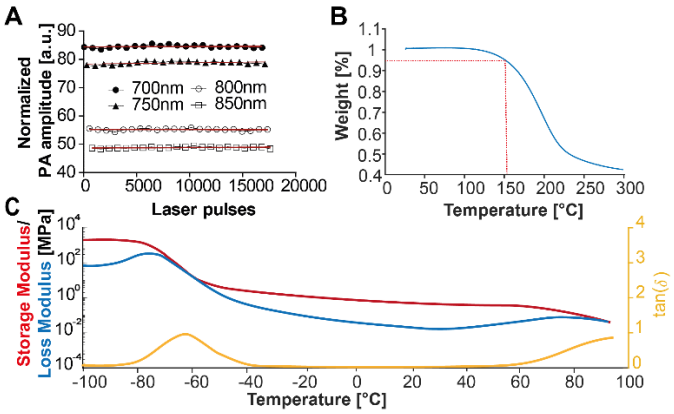

Fig. 4. **Photo and thermomechanical stability of the phantom material**. (A) When exposed to up to 17,500 laser pulses in the range of 700 nm to 850 nm (10 nm steps) within a PAI system, no significant change in the normalised photoacoustic signal amplitudes could be detected, representatively shown here for 700 nm (black circle), 750 nm (black triangle), 800 nm (white circle) and 850 nm (white square). Using a sample composed of mineral oil containing 30 w/v% high MW SEBS and 8 w/v% LDPE, a thermogravimetric (B) and dynamic mechanical analysis (C) were performed. The thermogravimetric test revealed 95 % weight preservation up to a temperature of 152 °C, denoted by the red dashed line. The sample was found to be stable in a range of −60 to 60 °C by dynamic mechanical analysis. The storage modulus E' is depicted in red, the loss modulus E" in blue and the damping factor tan(δ) (E"/E') in yellow.

absorption, respectively. When selecting the concentrations of TiO_2 and Nigrosin, we aimed to achieve μ_a and μ_s' values in the lower range of soft tissues, such as breast fat (μ_s' = 0.3-0.8 mm^{-1}; μ_a = 0.005-0.03 mm^{-1}) [62], but higher values can be easily achieved by increasing the concentration of TiO_2 and/or absorbing dye. The addition of TiO_2 resulted in a linear increase in scattering (Figure 3C), whilst addition of Nigrosin led to a linear increase in absorption (Figure 3D). The optical adjustment did not significantly affect the speed of sound (p = 0.2204) or the acoustic attenuation (p = 0.3159) of the sample. These results suggest that the optical characteristics of the proposed material can be independently tuned and adapted to any soft tissue type of interest.

C. The Copolymer-in-Oil Material Demonstrates Good Photo and Thermomechanical Stability

With the use of pulsed lasers in PAI, it is important to test whether a material can withstand photobleaching during laser illumination. Firstly, we evaluated the photostability of the phantom material and exposed it to 17,500 laser pulses in the wavelength range of 700 to 850 nm in a time frame of 30 minutes (Figure 4A). No significant change (slope: 0.000016 ± 0.000017, p = 0.4147) was observed in the normalized photoacoustic amplitude, indicating that our material is photostable for at least that exposure period.

Since many PAI systems can be expected to operate over a wide range of temperatures and copolymer-in-oil materials have previously shown a tendency to deform at elevated temperatures, we also assessed thermomechanical stability of our material, which incorporates a second polymer for increased mechanical stability. In order to assess thermostability, we conducted a thermogravimetric analysis for one representative formulation containing 8 w/v% LDPE and found less than 5% weight loss up to 152°C, suggesting that no major irreversible degradation occurs up to this temperature (Figure 4B). For assessment of the viscoelastic properties, we conducted a dynamic mechanical analysis (Figure 4C). We found the material to be stable from −63°C (= glass temperature T_g) to 60°C, which covers well the relevant working range of 20 to 40°C. The storage modulus for this representative formulation varied in this range between 0.44 (at 20°C) and 0.39 MPa (at 40°C), which resembles elastic values of stiffer soft tissue types (e.g. meniscus (0.3-0.8 MPa) [63].

D. Defined Acoustic and Optical Properties in the Material Are Repeatable and Temporally Stable

Copolymer-in-oil materials based on thermoplastic elastomers are thermo-reversible, allowing the material to be recast. Recasting affords the opportunity to prepare large batches of material that can later be formed into specific phantom objects with different geometries. Thus, we evaluated whether recasting affects the intrinsic properties of the material and found the impact to be minimal: for the acoustic properties, mean COVs of 0.010 ± 0.005 % (over n = 3) for the speed of sound and 3.1 ± 1.8 % for the acoustic attenuation could be measured in a frequency range of 2 to 10 MHz. For the optical properties, mean COVs of 7.5 ± 0.2 % for the measured transmission spectra and 2.1 ± 0.1 % for the reflectance spectra could be determined in a wavelength range of 450 to 900 nm.

Having the main constituents of the phantom material established, we also tested the intra-centre repeatability of our recipe by comparing the acoustic and optical properties of three independently fabricated samples made by the same operator at the same site (Department of Physics, University of Cambridge). The acoustic repeatability was found to be excellent with a mean COV of 0.03 ± 0.002 % for the speed of sound and 3.1 ± 1.3 % for the acoustic attenuation in a frequency range of 2 to 10 MHz. For the optical properties, repeatability was also found to be in an acceptable range, with COVs of 2.6 ± 0.005 % for the measured transmission spectra and 2.7 ± 0.001 % for the reflectance spectra in a wavelength range of 450 to 900 nm.

Finally, we assessed the long-term stability of the acoustic and optical properties of our phantom material. Acoustic and optical measurements were undertaken regularly over a time frame of eleven months. Linear fits gave slopes of 0.0014 ± 0.0043 $m{\cdot}s^{-1}$ for the speed of sound (Figure 5A), 0.00030 ± 0.00019 $dB{\cdot}cm^{-1}$ for the acoustic attenuation (Figure 5B), 0.00044 ± 0.00038 mm^{-1} for the reduced scattering coefficient (Figure 5C) and 0.0010 ± 0.0013 mm^{-1} for the optical absorption coefficient (Figure 5D). The slopes were not significantly non-zero (c(1): p = 0.77; α(1): p = 0.21; μ_s': p = 0.27, μ_a: p = 0.45), suggesting stability of the acoustic and optical properties over the investigated time frame. These findings taken together indicate a high repeatability of the material properties after recasting, with replicate fabrications and over time, supporting the potential of the material for use as a PAI phantom.

E. Phantom Design and Field Testing

For field-testing of our material, system-specific phantom designs for two distinct PAI systems were created. For the

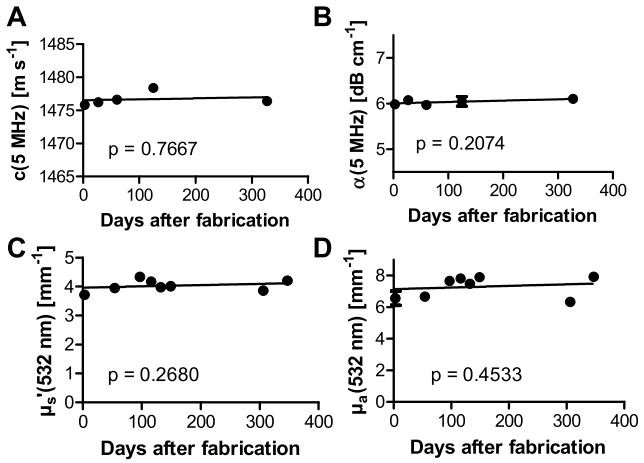

Fig. 5. **Stability of the acoustic and optical properties of the copolymer-in-oil material over time**. The speed of sound (A), acoustic attenuation (B), optical scattering coefficient (μ_s') (C) and optical absorption coefficient (μ_a) (D) of a material sample composed of 30 w/v% high MW SEBS, 8 w/v% LDPE, 0.03 w/v% TiO_2 and 0.0007 w/v% Nigrosin stock solution are shown over a time frame of eleven months. For all panels, data is shown as the mean ± SEM of n = 4 measurements per sample (error bars within symbols in all cases).

mesoscopic PAI system, a rectangular phantom was designed with three linearly spaced fibres embedded at specific depths (0.5, 1.5 and 2.5 mm) (Figure 6A, B) to test the homogeneity of the material in a high resolution PAI system and to evaluate how well targets of other materials could be embedded within the phantom material. The measured size of the fibre using PAI was found to correspond to the actual diameter of the fibre (average width of the signal peak 128 μm vs. 126 μm; Figure 6C, D). For the tomographic PAI system, a cylindrical phantom was created with two inclusions (diameter 4 mm) containing a green oil-soluble dye dissolved in the same base material (Figure 6E, F). The measured diameters extracted from the photoacoustic image were found to correspond with the designed dimensions of the phantom (outer part: 28 mm vs 27.7 ± 0.05 mm; inclusions: 4 mm vs 3.8 ± 0.07 mm and 3.8 ± 0.06 mm respectively, Figure 6G,H). Furthermore, the phantom was cut cross-sectionally at 6 months after formation and no diffusion of the dye from the inclusion to the background was observed. In both photoacoustic systems, the material appeared homogeneous and no distortions of the target dimensions were observed, supporting the suitability of the material for use in PAI.

IV. Discussion

PAI holds tremendous potential for clinical translation, but consensus performance test methods for quality assurance and control of PAI systems are still lacking. Moreover, quantitative performance evaluation of systems developed in different laboratories for different final applications remains a challenge. There is an urgent need to establish a PAI phantom material to support the standards development in the community; here, we have developed, optimised and extensively characterised a copolymer-in-oil phantom material to meet this need.

We focused initially on enhancing the tunability of acoustic properties in the tissue-mimicking range. By optimising the polymer composition and ratio, the speed of sound of the material was tuned to over 1500 m·s^{-1}, which is higher than described before in similarly composed materials [37], [38], [41], [42], [64], [65]. This allows the adaptation of the acoustic phantom properties to match those of tissues relevant for photoacoustic clinical applications, including breast tissue [66] and fat [45] (c = 1450 – 1480 m·s^{-1}; for LDPE concentrations 8 w/v %). Notably, LDPE concentrations over 20 w/v % should be avoided to prevent substantial elevation of acoustic attenuation. In particular, lower LDPE concentrations may be preferred for high frequency PAI systems and these can be easily fabricated by decreasing the polymer concentration, as shown for similar SEBS-based material recipes [41], [42]. Higher speed of sound values required for mimicking tissues such as muscle or kidney (>1520 m·s^{-1}; Supplementary Table I), could be achieved by choosing a plasticizer with higher viscosity [42] or by adding compounds such as glycerol [67], but these would lead respectively to higher acoustic attenuation [42] or acoustic backscattering [67], and reduced ease of the phantom fabrication. For independent tuning of acoustic backscattering properties, glass microspheres could be tested in future [38].

Having established an optimal acoustic composition for the material, we independently tuned the optical absorption and reduced scattering coefficients by the addition of oil-based inks and TiO_2. Here, Nigrosin was used as a representative absorber, but other photostable oil-soluble inks mimicking the absorption spectra of endogenous chromophores can be incorporated instead, as shown by Maneas *et al.* [37]. The high adaptability of both acoustic and optical properties supports the production of phantoms tailored to specific tissue types and applications of interest.

Further important criteria for a PAI phantom are photo- and thermomechanical stability of the intrinsic properties to enable reliable short- and long-term performance assessment of PAI systems. Our material was found to be photostable under the tested conditions and mechanically stable in the relevant working range of 20 to 40°C. It is known that the mechanical properties of copolymer-in-oil materials can be tuned in the tissue-mimicking range by adjusting the polymer concentration [42], [67]. The choice of plasticizer (e.g. viscosity, paraffinic content or molecular weight) also has been shown to affect the mechanical properties [68], [69]. While the adaptability to tissue-relevant mechanical properties has been shown for tissues with lower stiffness (2-150 kPa) [42], the material formulation tested here (with 8 w/v% LDPE) was found to be similar to tissues with higher stiffness, such as meniscus or soft tendons (0.3-0.8 MPa) [63] due to the higher polymer concentration used. The concomitant change of the acoustic and mechanical properties with adjustment of the polymer concentration needs to be considered by the user when choosing an appropriate formulation to use for their application. However, the adaptability of copolymer-in-oil materials to a wide range of tissue-relevant elasticities, as well as their large linear viscoelastic domain [42], make this class of material a promising candidate also for mechanically-relevant fields, such as ultrasound elastography [42], [70], [71]. We further demonstrated that our material can be used to create versatile phantom designs for PAI systems of different configurations.

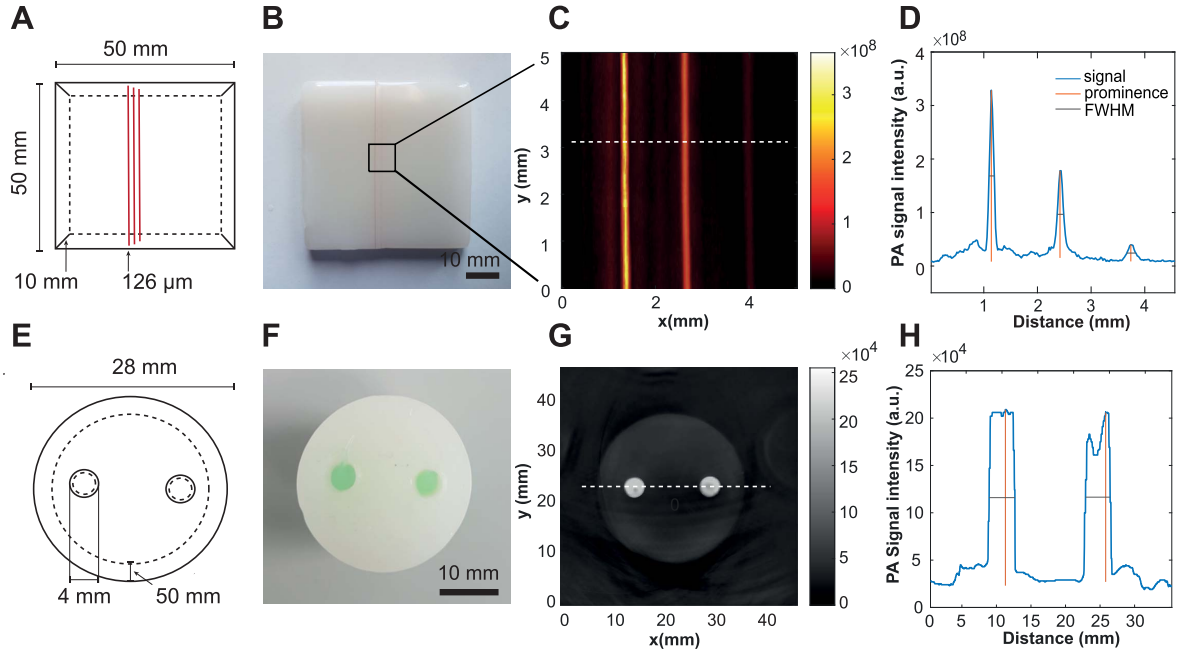

Fig. 6. **Copolymer-in oil material allows the creation of versatile phantom designs for different system configurations**. The design (A) and photograph (B) of a rectangular phantom for the mesoscopic system is shown. Three red fibres at different depths (0.5, 1.5 and 2.5 mm) act as imaging targets. (C) The photoacoustic x-y maximum intensity projection at 532 nm of the zoomed-in black square in (B) is displayed. (D) The intensity line profile of the white dotted line is shown (signal = blue, prominence = orange, width of signal peak at half maximum = grey). Correspondingly, the design (E), photograph (F) and photoacoustic image at 800 nm (G) of a cylindrical phantom for the tomographic system is shown. A green oil-soluble dye (GRC 43104; Caligo safe wash relief inks, Cranfield Colours, Cwmbran, UK) has been used as an absorber for the inclusions. (H) The intensity line profile of the white dotted line is shown (signal = blue, prominence = orange, width of signal peak at half maximum = grey).

The material showed high homogeneity during photoacoustic image acquisition and both endogenous inclusions made out of the same material type (as shown with the tomographic phantom) as well as exogenous targets (as shown with the mesoscopic phantom) can be embedded into the base matrix. Increasing polymer concentration increases the viscosity of the melt and the stiffness of the solidified material. This should be considered when fabricating phantoms containing small and delicate structures or inclusions, as for this purpose, a lower viscosity substance is preferable. Concomitantly, we observed that with increased viscosity the melt becomes less prone to air-bubble trapping, a problem observed in prior studies with lower viscosity copolymer-in-oil materials [38].

High reproducibility of the phantom fabrication procedure and ready availability of ingredients and equipment are further key requirements to enable widespread and comparable phantom manufacture in different laboratories. To optimise these parameters, we only chose non-toxic ingredients available from large scientific suppliers and simplified the fabrication procedure as far as possible while maintaining high manufacturing precision. A high intra-centre repeatability of the phantom fabrication procedure by the same operator was confirmed. Additionally, we showed that our material can be reused and remoulded without significantly affecting the acoustic and/or optical properties, which constitutes a further considerable advantage of the fabrication process. Importantly, we did not observe a statistically significant drift over a time frame of almost a year, thereby confirming expectations based on prior observations of longitudinal studies on the stability of oil-based materials [39]–[42]. Controllable mechanical robustness in the tissue-mimicking range and high intrinsic stability permit long-term usage of the material in a wide variety of phantom applications, which also has potential for application in biophotonic and ultrasound imaging.

While the reported material appears to be an excellent candidate for a PAI phantom to enable technical validation studies, there remain some limitations of our study. Firstly, we were unable to test the impact of including additives to tune acoustic backscattering due to limitations in our testing equipment. Secondly, we only performed fabrication and imaging studies in a single centre; future studies should also establish the inter-centre reproducibility to exclude the impact of variables such as equipment or operator. Moreover, we focused on an acoustic characterization in the clinically relevant range of 1-10 MHz. Future studies should also analyse the acoustic properties in a higher frequency range relevant for photoacoustic mesoscopy and microscopy. Finally, we generated only relatively basic performance assessment phantoms for PAI systems in our study. Increased anatomical realism may be achieved in future using 3D-printed moulds, potentially even with patient-derived vascular networks, as shown in similar studies [38], [72]–[74]. Preliminary tests indicate that our material is also 3D-printable, offering an even wider range of flexibility in terms of processing and fabrication.

V. Conclusion

We have optimised a copolymer-in-oil material and demonstrated its potential for use as a PAI phantom. The formulation presented holds significant promise for future adoption as a widespread phantom in PAI, with potential applications in

calibration, performance evaluation, and multi-centre standardisation of PAI systems, as well as for training of new users. Key beneficial properties of the material are:

i. tuneable and stable acoustic and optical properties;
ii. good mechanical, thermo- and photo-stability in the relevant working range;
iii. non-proprietary and non-toxic ingredients and
iv. high flexibility of phantom design and fabrication.

REFERENCES

[1] P. Beard, "Biomedical photoacoustic imaging," *Interface Focus*, vol. 1, no. 4, pp. 602–631, Aug. 2011, doi: 10.1098/rsfs.2011.0028.

[2] C. Li and L. V. Wang, "Photoacoustic tomography and sensing in biomedicine," *Phys. Med. Biol.*, vol. 54, no. 19, pp. R59–R97, Oct. 2009, doi: 10.1088/0031-9155/54/19/R01.

[3] A. B. E. Attia *et al.*, "A review of clinical photoacoustic imaging: Current and future trends," *Photoacoustics*, vol. 16, Dec. 2019, Art. no. 100144, doi: 10.1016/j.pacs.2019.100144.

[4] M. Heijblom, W. Steenbergen, and S. Manohar, "Clinical photoacoustic breast imaging: The twente experience," *IEEE Pulse*, vol. 6, no. 3, pp. 42–46, May 2015, doi: 10.1109/MPUL.2015.2409102.

[5] A. P. Regensburger *et al.*, "Detection of collagens by multispectral optoacoustic tomography as an imaging biomarker for duchenne muscular dystrophy," *Nature Med.*, vol. 25, no. 12, pp. 1905–1915, Dec. 2019, doi: 10.1038/s41591-019-0669-y.

[6] K. S. Valluru and J. K. Willmann, "Clinical photoacoustic imaging of cancer," *Ultrasonography*, vol. 35, no. 4, pp. 267–280, Oct. 2016, doi: 10.14366/usg.16035.

[7] D. J. Waterhouse, C. R. M. Fitzpatrick, B. W. Pogue, J. P. B. O'Connor, and S. E. Bohndiek, "A roadmap for the clinical implementation of optical-imaging biomarkers," *Nature Biomed. Eng.*, vol. 3, no. 5, pp. 339–353, May 2019, doi: 10.1038/s41551-019-0392-5.

[8] J. P. B. O'Connor *et al.*, "Imaging biomarker roadmap for cancer studies," *Nature Rev. Clin. Oncol.*, vol. 14, no. 3, pp. 169–186, Mar. 2017, doi: 10.1038/nrclinonc.2016.162.

[9] J. Laufer, E. Zhang, and P. Beard, "Evaluation of absorbing chromophores used in tissue phantoms for quantitative photoacoustic spectroscopy and imaging," *IEEE J. Sel. Topics Quantum Electron.*, vol. 16, no. 3, pp. 600–607, 2010, doi: 10.1109/JSTQE.2009.2032513.

[10] J. R. Cook, R. R. Bouchard, and S. Y. Emelianov, "Tissue-mimicking phantoms for photoacoustic and ultrasonic imaging," *Biomed. Opt. Exp.*, vol. 2, no. 11, p. 3193, Nov. 2011, doi: 10.1364/BOE.2.003193.

[11] W. Xia, D. Piras, M. Heijblom, W. Steenbergen, T. G. van Leeuwen, and S. Manohar, "Poly (vinyl alcohol) gels as photoacoustic breast phantoms revisited," *J. Biomed. Opt.*, vol. 16, no. 7, 2011, Art. no. 075002, doi: 10.1117/1.3597616.

[12] B. Amado-Rey, A. Mittnacht, and T. Stieglitz, "Experimental characterization of optoacoustic phantoms in gel wax and polyvinyl alcohol for blood pressure measurements," in *Proc. Annu. Int. Conf. IEEE Eng. Med. Biol. Soc. (EMBS)*, Jul. 2019, pp. 5820–5823, doi: 10.1109/EMBC.2019.8857175.

[13] E. Blumenröther, O. Melchert, M. Wollweber, and B. Roth, "Detection, numerical simulation and approximate inversion of optoacoustic signals generated in multi-layered PVA hydrogel based tissue phantoms," *Photoacoustics*, vol. 4, no. 4, pp. 125–132, Dec. 2016, doi: 10.1016/j.pacs.2016.10.002.

[14] A. Kharine *et al.*, "Poly (vinyl alcohol) gels for use as tissue phantoms in photoacoustic mammography," *Phys. Med. Biol.*, vol. 48, no. 3, pp. 357–370, Feb. 2003, doi: 10.1088/0031-9155/48/3/306.

[15] G. M. Spirou, A. A. Oraevsky, I. A. Vitkin, and W. M. Whelan, "Optical and acoustic properties at 1064 nm of polyvinyl chloride-plastisol for use as a tissue phantom in biomedical optoacoustics," *Phys. Med. Biol.*, vol. 50, no. 14, pp. N141–N153, Jul. 2005.

[16] S. E. Bohndiek, S. Bodapati, D. Van De Sompel, S.-R. R. Kothapalli, and S. S. Gambhir, "Development and application of stable phantoms for the evaluation of photoacoustic imaging instruments," *PLoS ONE*, vol. 8, no. 9, pp. 1–14, Sep. 2013, doi: 10.1371/journal.pone.0075533.

[17] M. Fonseca, B. Zeqiri, P. C. Beard, and B. T. Cox, "Characterisation of a phantom for multiwavelength quantitative photoacoustic imaging," *Phys. Med. Biol.*, vol. 61, no. 13, pp. 4950–4973, Jul. 2016, doi: 10.1088/0031-9155/61/13/4950.

[18] W. C. Vogt, C. Jia, K. A. Wear, B. S. Garra, and T. J. Pfefer, "Biologically relevant photoacoustic imaging phantoms with tunable optical and acoustic properties," *J. Biomed. Opt.*, vol. 21, no. 10, Oct. 2016, Art. no. 101405, doi: 10.1117/1.JBO.21.10.101405.

[19] M. Dantuma, R. van Dommelen, and S. Manohar, "Semi-anthropomorphic photoacoustic breast phantom," *Biomed. Opt. Exp.*, vol. 10, no. 11, pp. 5921–5939, Nov. 2019, doi: 10.1364/BOE.10.005921.

[20] E.-J. Jeong *et al.*, "Fabrication and characterization of PVCP human breast tissue-mimicking phantom for photoacoustic imaging," *BioChip J.*, vol. 11, no. 1, pp. 67–75, Mar. 2017, doi: 10.1007/s13206-016-1109-4.

[21] C. Jia, W. C. Vogt, K. A. Wear, T. J. Pfefer, and B. S. Garra, "Two-layer heterogeneous breast phantom for photoacoustic imaging," *J. Biomed. Opt.*, vol. 22, no. 10, pp. 1–14, Oct. 2017, doi: 10.1117/1.JBO.22.10.106011.

[22] C. Avigo *et al.*, "Organosilicon phantom for photoacoustic imaging," *J. Biomed. Opt.*, vol. 20, no. 4, Apr. 2015, Art. no. 046008, doi: 10.1117/1.JBO.20.4.046008.

[23] F. Ratto *et al.*, "Hybrid organosilicon/polyol phantom for photoacoustic imaging," *Biomed. Opt. Exp.*, vol. 10, no. 8, pp. 3719–3730, Aug. 2019, doi: 10.1364/BOE.10.003719.

[24] M. Firbank, M. Oda, and D. T. Delpy, "An improved design for a stable and reproducible phantom material for use in near-infrared spectroscopy and imaging," *Phys. Med. Biol.*, vol. 40, no. 5, pp. 955–961, May 1995, doi: 10.1088/0031-9155/40/5/016.

[25] J. C. Hebden, D. J. Hall, M. Firbank, and D. T. Delpy, "Time-resolved optical imaging of a solid tissue-equivalent phantom," *Appl. Opt.*, vol. 34, no. 34, pp. 8038–8047, Dec. 1995, doi: 10.1364/ao.34.008038.

[26] E. L. Madsen, M. A. Hobson, H. Shi, T. Varghese, and G. R. Frank, "Stability of heterogeneous elastography phantoms made from oil dispersions in aqueous gels," *Ultrasound Med. Biol.*, vol. 32, no. 2, pp. 261–270, Feb. 2006, doi: 10.1016/j.ultrasmedbio.2005.10.009.

[27] M. O. Culjat, D. Goldenberg, P. Tewari, and R. S. Singh, "A review of tissue substitutes for ultrasound imaging," *Ultrasound Med. Biol.*, vol. 36, no. 6, pp. 861–873, Jun. 2010, doi: 10.1016/j.ultrasmedbio.2010.02.012.

[28] K. Zell, J. I. Sperl, M. W. Vogel, R. Niessner, and C. Haisch, "Acoustical properties of selected tissue phantom materials for ultrasound imaging," *Phys. Med. Biol.*, vol. 52, no. 20, pp. N475–N484, Oct. 2007, doi: 10.1088/0031-9155/52/20/N02.

[29] M. Lazebnik, E. L. Madsen, G. R. Frank, and S. C. Hagness, "Tissue-mimicking phantom materials for narrowband and ultrawideband microwave applications," *Phys. Med. Biol.*, vol. 50, no. 18, pp. 4245–4258, Sep. 2005, doi: 10.1088/0031-9155/50/18/001.

[30] K. V. Ramnarine, T. Anderson, and P. R. Hoskins, "Construction and geometric stability of physiological flow rate wall-less stenosis phantoms," *Ultrasound Med. Biol.*, vol. 27, pp. 245–250, Feb. 2001, doi: 10.1016/S0301-5629(00)00304-5.

[31] B. W. Pogue and M. S. Patterson, "Review of tissue simulating phantoms for optical spectroscopy, imaging and dosimetry," *J. Biomed. Opt.*, vol. 11, no. 4, 2006, Art. no. 041102, doi: 10.1117/1.2335429.

[32] G. Lamouche *et al.*, "Review of tissue simulating phantoms with controllable optical, mechanical and structural properties for use in optical coherence tomography," *Biomed. Opt. Exp.*, vol. 3, no. 6, p. 1381, Jun. 2012, doi: 10.1364/BOE.3.001381.

[33] J. K. Tsou, J. Liu, A. I. Barakat, and M. F. Insana, "Role of ultrasonic shear rate estimation errors in assessing inflammatory response and vascular risk," *Ultrasound Med. Biol.*, vol. 34, no. 6, pp. 963–972, Jun. 2008, doi: 10.1016/j.ultrasmedbio.2007.11.010.

[34] M. M. Jalili, S. Y. Mousavi, and A. S. Pirayeshfar, "Investigating the acoustical properties of carbon fiber-, glass fiber-, and hemp fiber-reinforced polyester composites," *Polym. Compos.*, vol. 35, no. 11, pp. 2103–2111, Nov. 2014, doi: 10.1002/pc.22872.

[35] O. Fenollar, L. Sanchez-Nacher, D. Garcia-Sanoguera, J. López, and R. Balart, "The effect of the curing time and temperature on final properties of flexible PVC with an epoxidized fatty acid ester as natural-based plasticizer," *J. Mater. Sci.*, vol. 44, no. 14, pp. 3702–3711, Jul. 2009, doi: 10.1007/s10853-009-3495-7.

[36] U. Heudorf, V. Mersch-Sundermann, and J. Angerer, "Phthalates: Toxicology and exposure," *Int. J. Hygiene Environ. Health*, vol. 210, no. 5, pp. 623–634, Oct. 2007, doi: 10.1016/j.ijheh.2007.07.011.

[37] E. Maneas *et al.*, "Gel wax-based tissue-mimicking phantoms for multispectral photoacoustic imaging," *Biomed. Opt. Exp.*, vol. 9, no. 3, p. 1151, Mar. 2018, doi: 10.1364/BOE.9.001151.

[38] E. Maneas *et al.*, "Anatomically realistic ultrasound phantoms using gel wax with 3D printed moulds," *Phys. Med. Biol.*, vol. 63, no. 1, Jan. 2018, Art. no. 015033, doi: 10.1088/1361-6560/aa9e2c.

[39] C. J. M. Jones and P. R. T. Munro, "Stability of gel wax based optical scattering phantoms," *Biomed. Opt. Exp.*, vol. 9, no. 8, pp. 3495–3502, Aug. 2018, doi: 10.1364/BOE.9.003495.

[40] A. M. Ivory, A. Shah, S. Rajagopal, and B. Zeqiri, "Development and investigation of the acoustic properties of tissue-mimicking materials for photoacoustic imaging techniques," in *Proc. IEEE Int. Ultrason. Symp. (IUS)*, Oct. 2019, pp. 1489–1492, doi: 10.1109/ULTSYM.2019.8926203.

[41] L. C. Cabrelli, P. I. B. G. B. Pelissari, A. M. Deana, A. A. O. Carneiro, and T. Z. Pavan, "Stable phantom materials for ultrasound and optical imaging," *Phys. Med. Biol.*, vol. 62, no. 2, pp. 432–447, Jan. 2017, doi: 10.1088/1361-6560/62/2/432.

[42] J. Oudry, C. Bastard, V. Miette, R. Willinger, and L. Sandrin, "Copolymer-in-oil phantom materials for elastography," *Ultrasound Med. Biol.*, vol. 35, no. 7, pp. 1185–1197, Jul. 2009, doi: 10.1016/j.ultrasmedbio.2009.01.012.

[43] A. Suzuki *et al.*, "Oil gel-based phantom for evaluating quantitative accuracy of speed of sound measured in ultrasound computed tomography," *Ultrasound Med. Biol.*, vol. 45, no. 9, pp. 2554–2567, Sep. 2019, doi: 10.1016/j.ultrasmedbio.2019.05.011.

[44] H. E. Legge, N. R. Holden, and G. Schroeder, *Thermoplastic Elastomers*, 2nd ed. Munich, Germany: Hanser, 1996.

[45] T. L. Szabo, "Diagnostic ultrasound imaging—Inside out," in *Diagnostic Ultrasound Imaging*. Amsterdam, The Netherlands: Elsevier, 2004, pp. 243–295.

[46] N. S. Allen *et al.*, "Degradation and stabilisation of styrene–ethylene–butadiene–styrene (SEBS) block copolymer," *Polym. Degradation Stability*, vol. 71, no. 1, pp. 113–122, Jan. 2000, doi: 10.1016/S0141-3910(00)00162-2.

[47] B. Zeqiri, W. Scholl, and S. P. Robinson, "Measurement and testing of the acoustic properties of materials: A review," *Metrologia*, vol. 47, no. 2, pp. S156–S171, Apr. 2010, doi: 10.1088/0026-1394/47/2/S13.

[48] S. Rajagopal, N. Sadhoo, and B. Zeqiri, "Reference characterisation of sound speed and attenuation of the IEC agar-based tissue-mimicking material up to a frequency of 60 MHz," *Ultrasound Med. Biol.*, vol. 41, no. 1, pp. 317–333, Jan. 2015, doi: 10.1016/j.ultrasmedbio.2014.04.018.

[49] J. M. M. Pinkerton, "The absorption of ultrasonic waves in liquids and its relation to molecular constitution," *Proc. Phys. Soc. Sect. B*, vol. 62, no. 2, pp. 129–141, Feb. 1949, doi: 10.1088/0370-1301/62/2/307.

[50] J. W. Pickering, S. A. Prahl, N. van Wieringen, J. F. Beek, H. J. C. M. Sterenborg, and M. J. C. van Gemert, "Double-integrating-sphere system for measuring the optical properties of tissue," *Appl. Opt.*, vol. 32, no. 4, pp. 399–410, Feb. 1993, doi: 10.1364/AO.32.000399.

[51] E. Oregon Tech and A. Sw Parkway. (2011). *Everything I Think you Should Know About Inverse Adding-Doubling*. Accessed: Apr. 28, 2019. [Online]. Available: http://omlc.org

[52] M. Bakaric, A. Ivory, B. Zeqiri, B. T. Cox, and B. E. Treeby, "Measurement of the temperature-dependent speed of sound and change in Grüneisen parameter of tissue-mimicking materials," in *Proc. IEEE Int. Ultrason. Symp. (IUS)*, Oct. 2019, pp. 1–4, doi: 10.1109/ULTSYM.2019.8925838.

[53] A. Dima, N. C. Burton, and V. Ntziachristos, "Multispectral optoacoustic tomography at 64, 128, and 256 channels," *J. Biomed. Opt.*, vol. 19, no. 3, Mar. 2014, Art. no. 036021, doi: 10.1117/1.JBO.19.3.036021.

[54] D. Montalvão, R. A. L. D. Cláudio, A. M. R. Ribeiro, and J. Duarte-Silva, "Experimental measurement of the complex Young's modulus on a CFRP laminate considering the constant hysteretic damping model," *Compos. Struct.*, vol. 97, pp. 91–98, Mar. 2013.

[55] R. Kishimoto *et al.*, "Measuring shear-wave speed with point shear-wave elastography and MR elastography: A phantom study," *BMJ Open*, vol. 7, no. 1, Jan. 2017, Art. no. e013925.

[56] L. F. Nielsen, N. J. Wismer, and S. Gade, "Improved method for complex modulus estimation," Appl. Note, Brüel Kjær, Nærum, Denmark, 1996. [Online]. Available: https://orbit.dtu.dk/en/publications/improved-method-for-complex-modulus-estimation

[57] N. Özkaya, D. Leger, D. Goldsheyder, and M. Nordin, *Fundamentals of Biomechanics: Equilibrium, Motion, and Deformation*. Berlin, Germany: Springer, 2016.

[58] J. Joseph, M. R. Tomaszewski, I. Quiros-Gonzalez, J. Weber, J. Brunker, and S. E. Bohndiek, "Evaluation of precision in optoacoustic tomography for preclinical imaging in living subjects," *J. Nucl. Med.*, vol. 58, no. 5, pp. 807–814, May 2017, doi: 10.2967/jnumed.116.182311.

[59] R. W. Nunes, J. R. Martin, and J. F. Johnson, "Influence of molecular weight and molecular weight distribution on mechanical properties of polymers," *Polym. Eng. Sci.*, vol. 22, no. 4, pp. 205–228, Mar. 1982, doi: 10.1002/pen.760220402.

[60] A. J. F. Carvalho, "Caracterização de géis termorreversíveis de SEBS," *Polímeros*, vol. 10, no. 1, pp. 1–7, Mar. 2000, doi: 10.1590/s0104-14282000000100003.

[61] J. L. Sandell and T. C. Zhu, "A review of *in-vivo* optical properties of human tissues and its impact on PDT," *J. Biophotonics*, vol. 4, nos. 11–12, pp. 773–787, Nov. 2011, doi: 10.1002/jbio.201100062.

[62] S. L. Jacques, "Optical properties of biological tissues: A review," *Phys. Med. Biol.*, vol. 58, no. 11, pp. R37–R61, Jun. 2013, doi: 10.1088/0031-9155/58/11/R37.

[63] O. Chaudhuri, J. Cooper-White, P. A. Janmey, D. J. Mooney, and V. B. Shenoy, "Effects of extracellular matrix viscoelasticity on cellular behaviour," *Nature*, vol. 584, no. 7822, pp. 535–546, Aug. 2020, doi: 10.1038/s41586-020-2612-2.

[64] S. L. Vieira, T. Z. Pavan, J. E. Junior, and A. A. O. Carneiro, "Paraffin-gel tissue-mimicking material for ultrasound-guided needle biopsy phantom," *Ultrasound Med. Biol.*, vol. 39, no. 12, pp. 2477–2484, Dec. 2013, doi: 10.1016/j.ultrasmedbio.2013.06.008.

[65] F. Grillo *et al.*, "White-silicone rubber and copolymer-in-oil blend for ultrasound soft tissue mimicking material," in *Proc. IEEE Int. Ultrason. Symp. (IUS)*, Sep. 2017, pp. 1–4, doi: 10.1109/ULTSYM.2017.8092022.

[66] B. Rajagopalan, J. F. Greenleaf, P. J. Thomas, S. A. Johnson, and R. C. Bahn, "Variation of acoustic speed with temperature in various excised human tissues studied by ultrasound computerized tomography," in *Ultrasonic Tissue Characterization II*, vol. 525, M. Linzer, Ed. Washington, DC, USA: National Bureau of Standards, 1979, p. 227. [Online]. Available: https://books.google.co.uk/books?hl=en&lr=&id=AL7AirGJZfkC&oi=fnd&pg=PA227&ots=R-jtHXIpyP&sig=fdqo7uu_u28fTLACfr7-jCaIP-k&redir_esc=y#v=onepage&q&f=false

[67] L. C. Cabrelli, F. W. Grillo, D. R. T. Sampaio, A. A. O. Carneiro, and T. Z. Pavan, "Acoustic and elastic properties of glycerol in oil-based gel phantoms," *Ultrasound Med. Biol.*, vol. 43, no. 9, pp. 2086–2094, Sep. 2017, doi: 10.1016/j.ultrasmedbio.2017.05.010.

[68] M. M. Nguyen, S. Zhou, J.-L. Robert, V. Shamdasani, and H. Xie, "Development of oil-in-gelatin phantoms for viscoelasticity measurement in ultrasound shear wave elastography," *Ultrasound Med. Biol.*, vol. 40, no. 1, pp. 168–176, Jan. 2014, doi: 10.1016/j.ultrasmedbio.2013.08.020.

[69] J. K. Kim, M. A. Paglicawan, and M. Balasubramanian, "Viscoelastic and gelation studies of SEBS thermoplastic elastomer in different hydrocarbon oils," *Macromol. Res.*, vol. 14, no. 3, pp. 365–372, Jun. 2006, doi: 10.1007/BF03219096.

[70] J. Oudry, J. Chen, K. J. Glaser, V. Miette, L. Sandrin, and R. L. Ehman, "Cross-validation of magnetic resonance elastography and ultrasound-based transient elastography: A preliminary phantom study," *J. Magn. Reson. Imag.*, vol. 30, no. 5, pp. 1145–1150, Nov. 2009, doi: 10.1002/jmri.21929.

[71] E. Nicolas, S. Callé, and J.-P. Remenieras, "Generating shear waves in the human brain for ultrasound elastography: A new approach," *Phys. Procedia*, vol. 70, pp. 1255–1259, Jan. 2015, doi: 10.1016/j.phpro.2015.08.279.

[72] F. W. Grillo *et al.*, "Patient-specific neurosurgical phantom: Assessment of visual quality, accuracy, and scaling effects," *3D Printing Med.*, vol. 4, no. 1, pp. 1–9, Dec. 2018, doi: 10.1186/s41205-018-0025-8.

[73] D. I. Nikitichev, A. Barburas, K. McPherson, J.-M. Mari, S. J. West, and A. E. Desjardins, "Construction of 3-dimensional printed ultrasound phantoms with wall-less vessels," *J. Ultrasound Med.*, vol. 35, no. 6, pp. 1333–1339, Jun. 2016, doi: 10.7863/ultra.15.06012.

[74] S. J. West *et al.*, "Development of an ultrasound phantom for spinal injections with 3-dimensional printing," *Regional Anesthesia Pain Med.*, vol. 39, no. 5, pp. 429–433, 2014, doi: 10.1097/AAP.0000000000000136.